CMS Physics Analysis Summary

Contact: cms-pag-conveners-higgs@cern.ch 2024/03/26

Model-independent search for pair production of new bosons decaying into muons in proton-proton collisions at $\sqrt{s} = 13$ TeV

The CMS Collaboration

Abstract

The results of a model-independent search for the pair production of new bosons within a mass range of $0.21 < m < 60$ GeV, are presented. This study utilizes events featuring four muons in the final state and a dataset, comprising 41.5 fb^{-1} and 59.7 fb^{-1} of proton-proton collisions at $\sqrt{s} = 13$ TeV, recorded in 2017 and 2018 by the CMS experiment at the CERN LHC. The study of the 2018 dataset includes a search for displaced signatures of a new boson within the lifetime range of $0 < c\tau < 100$ mm. The results are combined with a prior CMS result, based on 35.9 fb^{-1} of proton-proton collisions at $0 < c\tau < 100$ mm collected in 2016. No significant deviation from the expected background is observed. Results are presented in terms of a model-independent upper limit on the product of cross section, branching fraction, and acceptance. The findings are interpreted across various benchmark models, such as an axion-like particle model, a vector portal model, the next-to-minimal supersymmetric standard model, and dark SUSY models, including those predicting a non-negligible lifetime of the new boson. In all considered scenarios, substantial portions of the parameter space are excluded, expanding upon prior results.

1 Introduction

Although the standard model (SM) [1–3] of particle physics provides a multitude of high-precision predictions consistent with decades of experimental results, it does not explain the existence of dark matter [4, 5]. Many models have been proposed that predict new bosons as dark matter candidates [6–8]. To date, no direct experimental evidence has yet materialized for particles beyond the SM (BSM), and in that context the idea of new bosons with non-negligible lifetimes [9], is of increasing interest. In this note, we present a model-independent search for the pair production of a new boson that decays into a pair of oppositely charged muons. This can happen in proton-proton (pp) collisions as $\mathrm{pp} \to 2a + \mathrm{X} \to 4\mu + \mathrm{X}$, where a is the new neutral boson and X are possible spectator particles [10]. The new boson a can be produced via various "portals" such as a Higgs boson (h) portal (either SM or non-SM) or a vector boson portal. Here, the production vertices of dimuons, i.e., pairs of oppositely-charged muons in the final state, can be either prompt or displaced. The displaced case results from the decays of long-lived BSM bosons. This generic signature enables us to set a model-independent limit on the product of the new boson production cross section, branching fraction to muons squared, and acceptance. This limit can then be interpreted in models with that final state.

We interpret the model-independent results in the context of several BSM benchmarks, including an axion-like particle (ALP) model [7, 11–14], a vector portal model with a dark scalar boson s_D [15–20], the next-to-minimal supersymmetric standard model (NMSSM) [6, 21–28], and supersymmetry (SUSY) models with hidden sectors (dark SUSY) [8, 20, 29]. In the ALP model [13], the SM-like Higgs boson h decays to the ALP a, via $\mathrm{h} \to 2a$. The ALP then promptly decays into a dimuon. In the vector portal model, a massive dark vector boson Z_D decays to two new scalar bosons s_D, via $Z_\mathrm{D} \to s_\mathrm{D}\overline{s_\mathrm{D}}$, where we assume that the s_D is not self-conjugate. The scalar boson s_D promptly decays to a dimuon. In the NMSSM, two of the three charge parity (CP) even neutral Higgs bosons h_1 or h_2 (generically denoted by $\mathrm{h}_{1,2}$) can decay to one of the two CP odd neutral Higgs bosons a_1 via $\mathrm{h}_{1,2} \to 2a_1$. The CP-odd boson a_1 promptly decays to a dimuon. In the dark SUSY scenario, the breaking of a new $U(1)_\mathrm{D}$ symmetry gives rise to a massive dark photon γ_D. This dark photon can couple to SM photons via a small kinetic mixing parameter (ε). The lifetime of the dark photon depends on its mass, m_{γ_D}, and ε. We use a signal topology where an SM-like h decays to the lightest non-dark neutralino n_1 via $\mathrm{h} \to 2\mathrm{n}_1$. These neutralinos then decay via $\mathrm{n}_1 \to \mathrm{n}_\mathrm{D} + \gamma_\mathrm{D}$, where n_D is an undetectable dark neutralino. The dark photon γ_D then decays to a dimuon.

The search presented in this note is improved compared to the previous result published by the CMS Collaboration in Ref. [30]. Compared to this study, we add more data and add two new benchmark models (the vector portal and ALP models), and probe a larger mass range of the new, neutral boson a ($0.21 < m_a < 60$ GeV, compared to $0.25 < m_a < 8.5$ GeV in Ref. [30]). Other searches at the LHC for $\mathrm{h} \to 2a$ include the 4e [31], 4μ [30, 32–35], 4τ [36, 37], 4ℓ [38–40], $4\ell/4\pi$ [31], $4\ell/8\ell$ [41], 4b [42, 43], 4γ [44], 2b 2τ [45], 2μ 2τ [46, 47], and 6q [48] final states. This model-independent analysis considers both promptly-decaying and long-lived ($c\tau < 100\,\mathrm{mm}$) muons and is complementary in exploring ε to other searches for promptly-decaying [49, 50] and long-lived [51, 52] muons.

Two datasets are used for this analysis, including data collected using multiple triggers in 2017 and 2018. These datasets correspond to integrated luminosities of 41.5 and 59.7 fb^{-1} of pp collisions at a center-of-mass energy of $\sqrt{s} = 13\,\mathrm{TeV}$, respectively. We present separate results of two combinations of these datasets; the first considers a combination of the 2017 and 2018 datasets, which correspond to a total integrated luminosity of $101\,\mathrm{fb}^{-1}$ the novel result of this study, and the second corresponds to the combination of the aforementioned datasets with a

previously published analysis which examined the 2016 data taking period [30], and corresponds to a total integrated luminosity of 137 fb^{-1}.

The triggers used in this study include a double standalone (SA) muon trigger with a $p_{\text{T}} > 23\,\text{GeV}$ threshold based on the muon reconstruction algorithm that uses only muon detectors [53]. This trigger was operated in 2018 and is used in the 2018 analysis. This double SA muon trigger does not rely on a primary vertex (PV) constraint for the track fit and is sensitive to both prompt and displaced muons probed in this search. The PV is taken to be the vertex corresponding to the hardest scattering in the event, evaluated using tracking information alone [54]. There was no equivalent trigger in 2017, thereby eliminating the possibility of investigating displaced track and vertex signatures.

The CMS detector is improved in this data run with a new silicon pixel tracking detector [55] installed and commissioned in 2017 [56]. It features a larger detector volume with four layers in the barrel and three layers in the endcaps. Compared to the previous pixel detector, the innermost layer is positioned closer to the interaction point (IP) and the outermost layer is located farther from the IP. The new pixel detector can cope with a higher particle rate, which subsequently improves impact parameter resolution and increases the tracking efficiency. The performance of the hardware trigger algorithms for muons is also improved [57]. The analysis criteria are modified to accommodate the search in an extended model parameter space as compared to Ref. [30]. New benchmark models are added to further test the model independence and diversify the interpretation.

This note is organized as follows: First, we discuss the layout and operation of the CMS detector in Section 2. Next, we review the simulation of signal samples in Section 3, event selection criteria in Section 4, and signal shape modeling in Section 5. We then present the processes of background estimation in Section 6 followed by an enumeration of the systematic uncertainties in Section 7. Finally, we provide the results of this analysis in Section 8, which is followed by a brief summary in Section 9.

2 The CMS detector

The central feature of the CMS apparatus is a superconducting solenoid of 6 m internal diameter, providing a magnetic field of 3.8 T. Within the solenoid volume are a silicon pixel and strip tracker, a lead tungstate crystal electromagnetic calorimeter (ECAL), and a brass and scintillator hadron calorimeter (HCAL), each composed of a barrel and two endcap sections. Forward calorimeters extend the pseudorapidity coverage provided by the barrel and endcap detectors. Muons are measured in gas-ionization detectors embedded in the steel flux-return yoke outside the solenoid.

Muons are measured in the pseudorapidity range $|\eta| < 2.4$, with detection planes made using three technologies: drift tubes, cathode strip chambers, and resistive plate chambers. The single muon trigger efficiency exceeds 90% over the full η range, and the efficiency to reconstruct and identify muons is greater than 96%. Matching muons to tracks measured in the silicon tracker results in a relative transverse momentum (p_{T}) resolution—for muons with p_{T} up to 100 GeV, a relative transverse momentum resolution of 1% in the barrel and 3% in the endcaps. The p_{T} resolution in the barrel is better than 7% for muons with p_{T} up to 1 TeV [53].

Events of interest are selected using a two-tiered trigger system [58]. The first level (L1), is composed of custom hardware processors, and uses information from the calorimeters and muon detectors to select events at a rate of around 100 kHz within a fixed time interval of about

4 μs. The second level, known as the high-level trigger (HLT), consists of a farm of processors running a version of the full event reconstruction software optimized for fast processing. The HLT further reduces the event rate to around 1 kHz before the data are sent for permanent storage [58].

A more detailed description of the CMS detector, together with a definition of the coordinate system used and the relevant kinematic variables, can be found in Ref. [59].

3 Benchmark signal models

Simulated signal events are generated with Monte Carlo (MC) simulations and are used to determine the effect of the data selection criteria (described in Section 4) on the various signal models. In the ALP model, production of the SM-like h via gluon-gluon (gg) fusion and its subsequent decays are simulated at next-to-leading order (NLO) with the matrix-element generator MADGRAPH5_aMC@NLO 2.4.2 [60, 61]. The mass of the SM-like h is fixed to 125 GeV and masses between 0.5 and 30 GeV for the ALP are simulated. For the vector portal model, production of the spin-1 Z_D and its subsequent decays are simulated at NLO with MADGRAPH5_aMC@NLO 2.6.5. Masses of the Z_D between 85 and 200 GeV are simulated, and the masses of the scalar boson s_D are simulated from 5 to 55 GeV depending on the kinematic constraints set by the Z_D mass.

In the case of the NMSSM, the production of the CP even $h_{1,2}$ via gg fusion and its decay to the CP odd a_1 is carried out at leading order with PYTHIA 8.230 [62]. Since the $h_{1,2}$ might not be the observed SM Higgs boson [63–65], mass values of $m_{h_{1,2}}$ between 90 and 150 GeV are simulated. This range is motivated by constraints set by the relic density measurements from WMAP [65], Planck [66], and searches at LEP [67–72]. The mass of the searched boson a_1 is set to vary between 0.5 and 3 GeV as motivated in Ref. [73].

In the dark SUSY model, production of the SM-like Higgs boson via gg fusion and its decays are simulated at NLO with MADGRAPH5_aMC@NLO 2.4.2. The masses of the SM Higgs boson, the neutralino n_1, and the dark neutralino n_D are fixed to 125, 60, and 1 GeV, respectively. Dark photon masses m_{γ_D} are simulated between 0.25 and 58 GeV, which are set to decay to a pair of oppositely charged muons 100% of the time. Since the dark photon interacts weakly with SM particles, its decay width is negligible compared to the dimuon mass resolution.

Discussed in greater detail in Section 4, we consider displaced tracks and vertices for the case of long-lived mediators in the 2018 analysis only. This decision results from the lack of triggers available for the 2017 dataset that are comparable to those used in the 2018 analysis for displaced signatures. When considering muon displacement for the 2018 analysis, we model the muon displacement in the lab frame via an exponential distribution with $c\tau_{\gamma_D}$ between 0 and 100 mm.

For all samples, pp collisions at 13 TeV are simulated using a set of parton distribution functions (PDFs) provided by NNPDF3.1 [74]. The parton shower, underlying event activity, and hadronization processes at the LHC are modeled with the MC event generator PYTHIA 8.230 using the CP5 tune [75]. All MC generated events are run through the full CMS simulation based on GEANT4 [76] and reconstructed with the same algorithms that are used for the data.

4 Event selection

Several triggers were used to collect the data used in this study, all with a total efficiency of more than 90% for all signal benchmarks described in Section 3. These include the double SA muon HLT mentioned in Section 1 and three extra triggers with relaxed p_T thresholds to improve the trigger efficiency on potential signals further.

For the 2017 dataset, we employ a double muon trigger with p_T thresholds of 23 and 12 GeV. Three other triggers with lower pT thresholds have been used to further improve the trigger efficiency on potential signals. Of these remaining triggers, we utilize a double muon trigger requiring muons of the same sign, with p_T thresholds of 18 and 9 GeV, a triple muon trigger with p_T thresholds of 12, 5, and 5 GeV, and a triple tracker muon trigger with pT thresholds of 12, 10, and 5 GeV. The tracker muon refers to muons identified using information from tracker tracks and typically matches only to segments in the innermost muon station [53].

The 2018 dataset retains the last three triggers used in the 2017 dataset but replaces the first trigger with one that is sensitive to displaced signatures. As such, the chosen double SA muon trigger requires at least two reconstructed muons in the muon detectors with a transverse momentum and pseudorapidity of $p_T > 23\,\text{GeV}$ and $|\eta| < 2$, respectively. This specific trigger was not available for the 2017 dataset; a study of the comparable double SA muon triggers available in 2018 either showed poor efficiencies for displaced muons in the pixel volume of the CMS experiment or negligible effective luminosities, thereby eliminating the use of these triggers in the 2017 analysis.

For both the 2017 and 2018 analyses, we require at least four offline reconstructed muons in each event. Among these muons, the 2017 analysis requires all muons to be reconstructed with the particle-flow (PF) algorithm [77], which performs a global fit that combines information from each subdetector, while the 2018 analysis requires at least three muons to be reconstructed with the PF algorithm and at most one SA muon reconstructed using only the information from the muon system. Selecting one possible SA muon in the 2018 analysis is necessary to mitigate lost efficiency for displaced muon reconstruction in the tracker. Each muon in the 2017 and 2018 analyses must have $p_T > 8\,\text{GeV}$ and $|\eta| < 2.4$. For the 2017 analysis, we require at least two high-p_T muons, i.e., muons with $p_T > 13\,\text{GeV}$. In the 2018 analysis, we require a higher threshold for these two high-p_T muons, with $p_T > 24\,\text{GeV}$. For the 2017 and 2018 analyses, we also require that these high-p_T muons are located in the region $|\eta| < 2$.

For both the 2017 and 2018 analyses the following selections are made: Any two oppositely charged muons in the event are paired as long as their invariant mass is below 60 GeV. The decay vertices of each dimuon in each event are reconstructed using the Kalman filtering (KF) technique [78], and only those vertices with a valid fitted vertex are retained. We further select two dimuons with the minimum difference between their invariant masses. These two dimuons must not have any muons in common with each other. A dimuon that does not contain a high-p_T muon is labeled a low-p_T dimuon (denoted as $\mu\mu_2$), while the other dimuon, which includes at least one high-p_T muon, is called a high-p_T dimuon (denoted as $\mu\mu_1$). In the scenario where both dimuons contain a high-p_T muon, the dimuons are randomly labeled to prevent bias in the kinematic distributions. All single muons not included in the two dimuons are called orphan muons. No requirements are applied to the orphan muons. We require that each of the two dimuons contain at least one muon that has at least one valid hit in any of the layers of the pixel detector. This requirement ensures the selected dimuons originate from the signal bosons that decay in the pixel detectors.

To further ensure that the signal muons in each dimuon decay from the same boson, we re-

quire a limit on the Kalman-fitted dimuon vertex probability, $P_{\mu\mu}$. For the 2017 analysis, this level is set to 15%. As the dimuon transverse displacement (L_{xy}) and the opening angle of the two muons $\left(\Delta R = \sqrt{(\Delta\eta)^2 + (\Delta\phi)^2}\right)$ increase, the fitted vertex probability decreases. As the 2018 analysis considers displaced signals, we account for this different probability threshold by defining a probability function which accepts L_{xy}, ΔR, and the number of SA muons, N_{SA}, and select valid fitted vertices based on the criterion $P_{\mu\mu} > P\left(L_{xy}, \Delta R, N_{\text{SA}}\right)$. To ensure uniform selection across 2017 and 2018 data, a minimum of 15% is set for the 2018 valid-vertices criterion. Finally, we place a selection on the transverse displacement of $L_{xy} < 16.0\,\text{cm}$.

We also require that each dimuon is sufficiently isolated by selecting dimuon pairs with a total isolation sum of less than 2.3 GeV. This isolation sum, $\text{Iso}_{\mu\mu}$, is calculated as the scalar sum of the transverse momenta of all reconstructed tracks with $p_{\text{T}} > 0.5\,\text{GeV}$ in the vicinity of the dimuon, i.e., within $\Delta R < 0.4$ and $|z_{\text{track}} - z_{\mu\mu}| < 0.1\,\text{cm}$. Here, z_{track} is defined as the z coordinate of the point of closest approach of the track to the primary vertex along the beam axis, while $z_{\mu\mu}$ is the z position of the vertex associated with the dimuon propagated back to the beamline along the dimuon direction vector. Tracks included in the dimuon reconstruction are excluded from the isolation calculation. Requiring $\text{Iso}_{\mu\mu} < 2.3\,\text{GeV}$ effectively removes about 72% of the quantum chromodynamic (QCD) background radiation. For a comprehensive and compact representation of all selection criteria, see Table 1.

Table 1: The event selection requirements for the 2017 and 2018 analyses. In the signal muon selection row, the particle-flow loose muons refer to those muons that have tracks in both the tracker and the muon system, which is contrasted with the standalone (SA) muon selection, which only requires tracks in the muon system.

Selection	Additional information	Requirement 2017	Requirement 2018
Signal muon candidates		4 PF loose muons	$\geq$3 PF loose muons and $\leq$1 SA muon
p_T ($\lvert\eta\rvert$)	2 signal muons	$p_T > 13\,\text{GeV}$ ($\lvert\eta\rvert < 2.0$)	$p_T > 24\,\text{GeV}$ ($\lvert\eta\rvert < 2.0$)
	All 4 signal muons	$p_T > 8\,\text{GeV}$ ($\lvert\eta\rvert < 2.4$)	$p_T > 8\,\text{GeV}$ ($\lvert\eta\rvert < 2.4$)
Invariant mass	Each dimuon	$m_{\mu\mu_i} < 60\,\text{GeV}$	$m_{\mu\mu_i} < 60\,\text{GeV}$
Fitted dimuon vertex probability	Each dimuon	$P_{\mu\mu_i} > 0.15$	$P_{\mu\mu_i} > P(L_{xy}, \Delta R, N_{\text{SA}})$
Dimuon isolation	Each dimuon	$\text{Iso}_{\mu\mu_i} < 2.3\,\text{GeV}$ ($\Delta R < 0.4$)	$\text{Iso}_{\mu\mu_i} < 2.3\,\text{GeV}$ ($\Delta R < 0.4$)
Fiducial volume	Each dimuon	N/A	$L_{xy} < 16.0\,\text{cm}$ $L_z < 51.6\,\text{cm}$

5 Signal shape modeling and signal region definition

The target new boson is presumed to be weakly coupled to SM particles with a narrow width; therefore, the shape of the dimuon invariant mass distribution is fully determined by the detector resolution and final-state radiation (FSR) from the muons.

The signal region (SR), defined by the signal mass window in the two-dimensional (2D) plane of $m_{\mu\mu_1}$ and $m_{\mu\mu_2}$ is determined by fitting the signal shape distributions of the MC signal samples with a double-sided Crystal Ball (CB) function (modified from [79] to include a tail on each side of the Gaussian function). This composite function consists of a Gaussian core and two power-law tails. The sigma parameter of the CB function describes the width of the Gaussian fit to the signal and, consequently, the signal resolution. To set the mass window size across

the signal mass phase space, we extract the sigma parameter from each fitted data point and plot it as a function of the invariant dimuon mass. To create a continuous signal mass window, we use the values obtained by linearly interpolating the plotted data points. Figure 1 displays the signal window mass size as a function of invariant dimuon mass (green dots) with the line derived from linear interpolation (dashed, purple line).

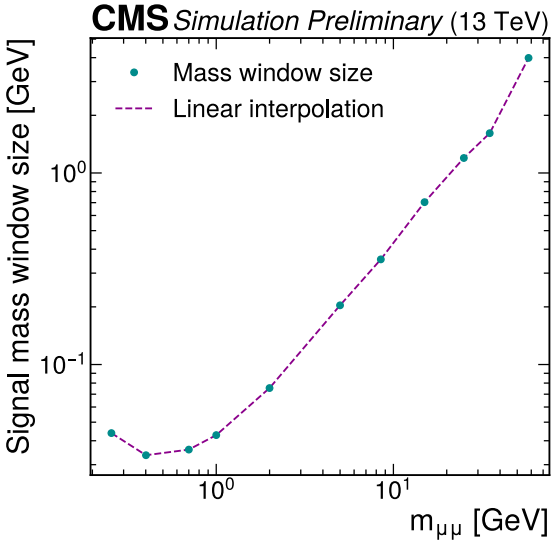

Figure 1: The mass window size as a function of invariant dimuon mass. It is derived from a Crystal Ball function fitting to MC signal events to contain 90% of events. The wider mass window size in $m \lessapprox 0.4\,\text{GeV}$ is due to deteriorating mass resolution for near-collinear dimuon in decays of low-mass boson.

Because the two dimuons originate from identical bosons, the signal mass window selection is motivated by the requirement of consistent invariant masses of the dimuons. This requirement is displayed in Equation (1) below,

$$|m_{\mu\mu_1} - m_{\mu\mu_2}| < W\big((m_{\mu\mu_1} + m_{\mu\mu_2})/2\big) \tag{1}$$

where W is a function of the dimuon invariant masses $m_{\mu\mu_1}$ and $m_{\mu\mu_2}$, and is based on the interpolation of the sigma parameters previously discussed. To determine the best signal significance, $S/\sqrt{S+B}$, where S is the signal and B is the expected background in the SR, thereby maximizing the discovery potential of this work, we examine the effect of four different signal efficiencies for prompt signals: 80%, 85%, 90%, and 95%.

For all signal efficiencies chosen, the signal significance decreases as the dimuon mass increases. However, over the entire mass range probed, $0.21 < m_{\mu\mu} < 60\,\text{GeV}$, a signal mass window providing a 90% efficiency on signal events yielded the best signal significance. Thus, given the combination of the mass window size and placement in the $(m_{\mu\mu_1}, m_{\mu\mu_2})$ mass phase-space, we achieve the greatest signal efficiency over the entire signal mass range, which we use here to define the SR. This selection ultimately carves out the signal region in the 2D plane of $m_{\mu\mu_1}$ and $m_{\mu\mu_2}$, as illustrated by the dashed lines in Figs. 2 and 3.

The model independence of the results in this search is confirmed by verifying that the ratio of the full reconstruction efficiency ϵ_{Full} over the generator level acceptance α_{Gen} is independent of all signal benchmarks. The acceptance α_{Gen} is defined as the fraction of MC-generated signal

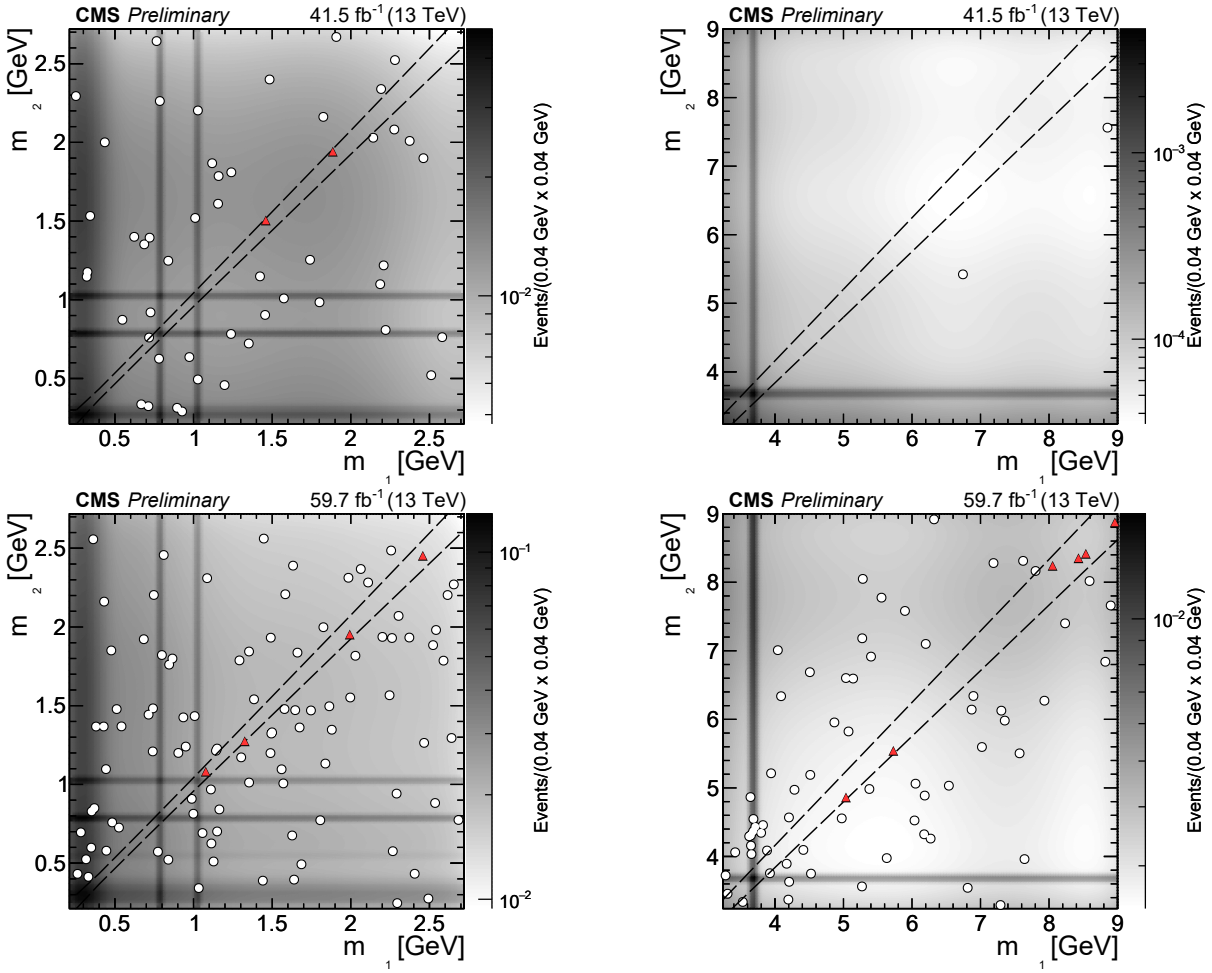

Figure 2: Two-dimensional distribution of the invariant masses $m_{\mu\mu_1}$ vs. $m_{\mu\mu_2}$ below (left) and above (right) the J/ψ resonance, for the 2017 (top row) and 2018 (bottom row) analyses. The grayscale heatmaps show the normalized QCD background templates. The white dots represent data events that pass all selection criteria but fall outside the SR $m_{\mu\mu_1} \simeq m_{\mu\mu_2}$ (outlined by dashed lines), and the red triangles represent data events passing all selection criteria. As discussed in Section 6.1, the paucity of events in the CR for the 2017 analysis, particularly the region above J/ψ, is a result of the triggers selected for this data-taking period.